Available online at www.sciencedirect.com

ScienceDirect

MATTER AND RADIATION AT EXTREMES

Matter and Radiation at Extremes 3 (2018) 135–144

www.journals.elsevier.com/matter-and-radiation-at-extremes

Research Article

Recent progress in ICF target fabrication at RCLF

Kai Du*, Meifang Liu, Tao Wang, Xiaoshan He, Zongwei Wang, Juan Zhang

Research Center of Laser Fusion, CAEP, P.O. Box 919-987, Mianyang, Sichuan 621900, China

Received 2 April 2017; revised 23 November 2017; accepted 15 December 2017
Available online 22 March 2018

Abstract

Target is one of the essential parts in inertial confinement fusion (ICF) experiments. To ensure the symmetry and hydrodynamic stability in the implosion, there are stringent specifications for the target. Driven by the need to fabricate the target required by ICF experiments, a series of target fabrication techniques, including capsule fabrication techniques and the techniques of target characterization and assembly, are developed by the Research Center of Laser Fusion (RCLF), China Academy of Engineering Physics (CAEP). The capsule fabrication techniques for preparing polymer shells, glow discharge polymer (GDP) shells and hollow glass micro-sphere (HGM) are studied, and the techniques of target characterization and assembly are also investigated in this paper. Fundamental research about the target fabrication is also done to improve the quality of the target. Based on the development of target fabrication techniques, some kinds of target have been prepared and applied in the ICF experiments.

PACS codes: 42.25.Hz; 64.70.pv; 68.05.Gh; 68.55.Ln; 81.15.Gh

Keywords: Capsule fabrication; Target characterization and assembly; Microencapsulation technique; Depolymerizable mandrel technique; White-light interferometry

1. Introduction

With increasing requirements of energy in the world, laser inertial confinement fusion (ICF), one of the most promising methods to control nuclear fusion reaction, have attracted a great deal of interest [1]. In ICF experiments, one essential part is the target, which usually consists of a spherical capsule with fuels inside and a hohlraum housing the capsule. For example, an indirect drive ICF experimental target is comprised of a microsphere filled with deuterium (DD) or deuterium-tritium (DT) fuel, and a metal cylindrical hohlraum converting laser radiation to X-ray which acts as the driver for fusion. It has been reported that the target quality is important to the symmetry and hydrodynamic stability in the implosion, so there are stringent specifications for the target [2,3]. Therefore, in order to meet these specifications, it is necessary to not only develop the capsule fabrication technique, but also explore the technology of the target characterization and assembly.

Over the past two decades, a lot of research work has been done, and a series of target techniques including capsule fabrication techniques and the techniques of target characterization and assembly are developed. In this paper, the capsule fabrication techniques for preparing polymer shells, glow discharge polymer (GDP) shells and hollow glass micro-sphere (HGM) are studied, along with the techniques of target characterization and assembly. Fundamental mechanisms about target fabrication are also discussed to improve target quality.

2. Capsule fabrication

2.1. Polymer shells prepared by microencapsulation technique

As we know, many kinds of polymer shells such as polystyrene (PS), deuterated PS, and poly(α-methylstyrene)

* Corresponding author.
E-mail address: icf802@163.com (K. Du).
Peer review under responsibility of Science and Technology Information Center, China Academy of Engineering Physics.

https://doi.org/10.1016/j.mre.2017.12.005

(PAMS) shells can be used for preparing the ICF targets [4,5]. Generally, these polymer shells are usually made by the microencapsulation technique, in which compound droplets consisting of three phases and two interfaces are prepared firstly, then the solvent in O phase and the core water is removed in the curing and dry process, respectively, forming shells. It has been reported that the generation of droplets can be controlled and manipulated systematically by developing kinds of microfluidics in recent years, which solve the formation problem of compound droplets [6–8]. However, there are stringent specifications on the shape of polymer shells used in ICF experiments, such as sphericity and wall thickness uniformity, since asymmetry and hydrodynamic instability would be exponentially amplified by any deviations from perfect sphericity, disrupting the ablation-driven implosion. The key constraint in sphericity and uniform wall thickness of the shells in turn requires a spherical and centered core compound droplet before its solidification. Therefore, how to precisely optimize the curing process to improve the quality of the polymer shells has been a challenge, especially for thick-walled polymer shells.

As shown in Fig. 1(a), the initial compound droplets are not perfectly spherical and concentric drops. It is found that there are many factors, such as density, interfacial tension, and viscosity, influencing the deformation of these droplets [9], but possible underlying mechanisms of these factors are not clear enough. Therefore, it is important to investigate the parameters on the deformation of these droplets.

In recent years, the effects of the density matching, interfacial tension, viscosity and continuing fluid field on the deformation have been investigated and some insights are obtained. The spherical driving force is from the interfacial tension affected by the two relative phases, while the concentric driving force is a resultant force, not only affected by the properties of the three phases, but also by the movement of the continuing fluid field. Therefore, increasing the interfacial tension provides an effective method to improve the sphericity. It has been proved that either replacing poly(vinyl alcohol) (PVA) with poly(acrylic acid) (PAA) or adding a small amount of hexadecane (H) into the oil phase (O) can increase the batch yield of PS shells with the out-of-round (δ_{OOR}) values less than 1 μm [10].

Compared with the sphericity, improving the wall uniformity is more challenging, since it is not only affected by the deformation of the middle phase, but also influenced by the movement of the internal phase. As shown in Fig. 2, with the density of the compound droplets being almost equal to or a little lower than that of the external phase, the gravity can be balanced by the buoyancy, so good dispersion and sufficient tumbling of the droplets could occur during the solidifying process, which improves the wall thickness uniformity [12]. Moreover, the viscous shear force plays a paradoxical role on the concentricity. Appropriate viscous shear force can center a compound droplet, while a too large viscous shear force can decenter it and decrease sphericity [13]. Therefore, optimizing the density matching, viscosity and continuing fluid field can improve wall thickness uniformity.

Based on the understanding of spherical and concentric mechanisms, as shown in Fig. 1(b), polymer shells with high sphericity and uniform wall thickness are obtained by increasing the interfacial tension, optimizing the density matching and the viscosity, and adjusting the continuing fluid field. With more stringent specifications required by ICF, more research is needed to be established in future, including fundamental studies of various subjects, for example, the effects of the interfacial tension on wall uniformity, the effects of the properties of the interfacial film such as interfacial film strength and interfacial rheology on the deformation, the balance between the centering and the deformation, and so on.

2.2. GDP shells prepared by plasma polymerization technology

To achieve ignition, the GDP shells must satisfy stringent specifications such as uniform wall thickness, smooth surface, wall compositional uniformity and so on [14]. The GDP shells are produced by plasma polymerization, in which hydrogen and trans-2-butene (T_2B) gases are broken down in an inductively coupled plasma system onto the surface of PAMS shells prepared by microencapsulation technique [15]. The deposition process is a key step in determination of the GDP properties. To date, there are much research on the relationship between deposition parameters and properties of the GDP shells [16–19]. However, little attention has been paid to the

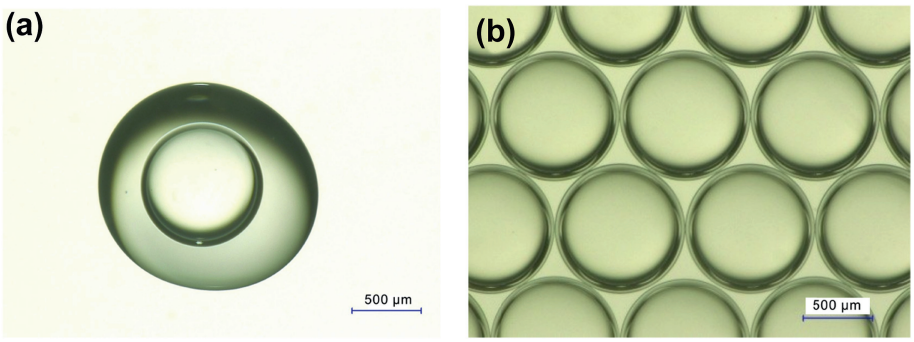

Fig. 1. Microphotographs of PS compound droplets and shells prepared by the microencapsulation technique: (a) PS compound droplets and (b) PS shells.

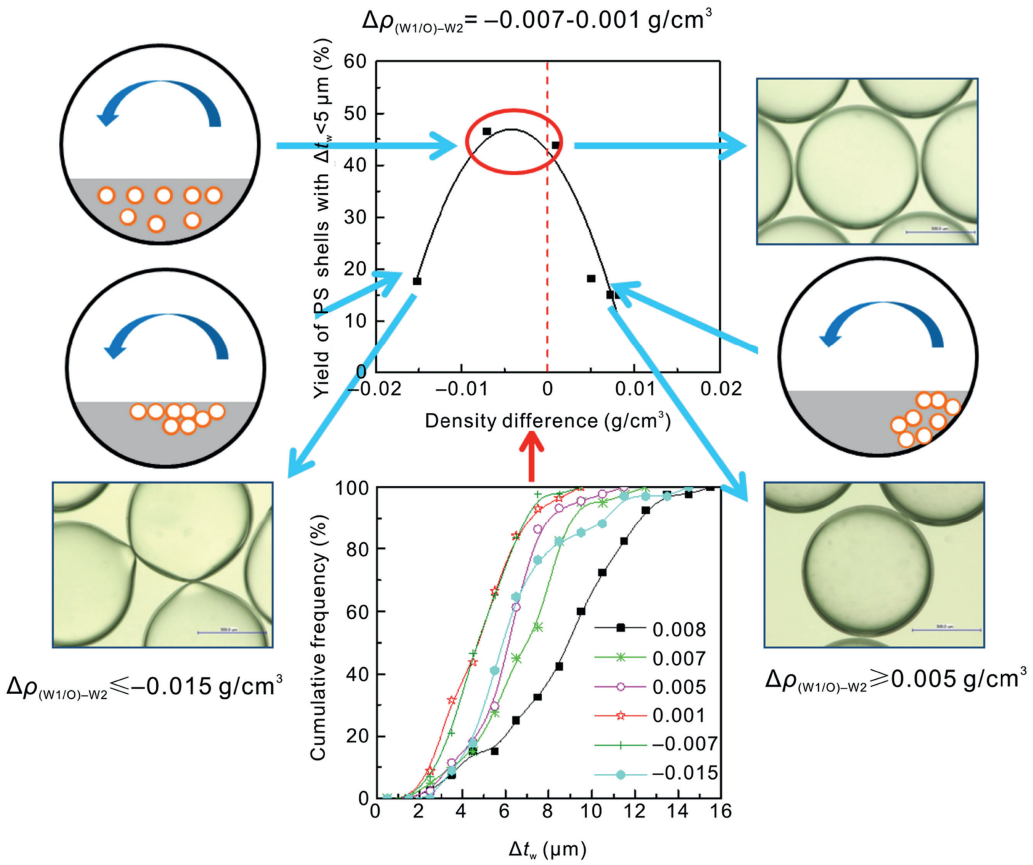

Fig. 2. Effects of the density matching level between compound droplets and external phase on the quality of polystyrene shells [11].

plasma for the process. Herein, the fundamental aspects of plasma for the GDP shells formation are discussed.

The mass spectrum of plasma for GDP deposition at different discharge powers has been analyzed, as shown in reference [20]. No trans-2-butene molecular peak at $m/e = 56$ is observed, so the amount of precursor is resolved as $C_2H_4^+$ ($m/e = 28$), $C_2H_6^+$ ($m/e = 30$), $C_3H_3^+$ ($m/e = 39$), $C_4H_5^+$ ($m/e = 53$), $C_5H_7^+$ ($m/e = 67$), $C_6H_9^+$($m/e = 81$), etc. It should be emphasized that the plasma consists of both large-mass species and small-mass species. This indicates that polymerization process in the gas phase following the initial decomposition of source molecules by electron collisions [21]. Besides, the molecules are dissociated more extensively with the increase of discharge power. Corresponding to the difference of hydrocarbon plasma, the GDP shell deposited at 10 W resembles cauliflower surface, while GDP shell deposited at 30 W becomes smooth and clear without pimples [20].

The mass spectrum of plasma at different gas mixture is analyzed, as shown in Fig. 3. The prominent mass peaks are $C_2H_4^+$($m/e = 28$), $C_2H_6^+$($m/e = 30$), $C_2H_8^+$($m/e = 32$), $C_3H_3^+$($m/e = 39$), $C_3H_8^+$($m/e = 44$), $C_5H_8^+$($m/e = 59$), etc. The intensity of hydrocarbon species increases with increasing gas flow ratio of T_2B/H_2. However, the relative intensity of small-mass species (for example $C_2H_6^+$ ($m/e = 30$)) increases more than that of the large-mass species. It is evident that the dissociated species with smaller-mass are more abundant at any case, especially at the gas flow ratio of 0.6:10. Because of the extensive dissociation, the surface roughness of the GDP shell decreases with the increasing gas flow ratio of T_2B/H_2 [22].

Moreover, in some implosion experiments, it is necessary to control preheat in ignition targets and the ablation front instability by doping the shells with a small quantity of high Z material, such as silicon and germanium [23,24]. The silicon-doped GDP deposition process is investigated by mass spectrum, as shown in Fig. 4(a). For comparison, the electron impact ionization of GDP deposition without tetramethyl silicon (TMS) gas is also analyzed, as shown in Fig. 4(b). There are many large-mass species when the silicon-doped GDP is

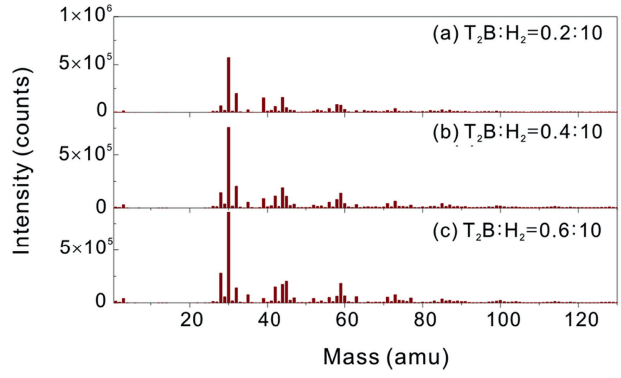

Fig. 3. Mass spectra of GDP deposition at different gas flow ratio.

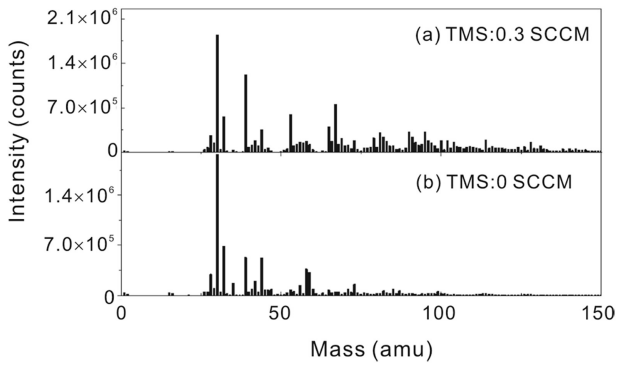

Fig. 4. Mass spectra of GDP deposition: (a) with TMS gas and (b) without TMS gas.

prepared. The large-mass species come from either the original TMS radicals or the SiC_xH_y radicals that might break into SiC_xH_{y-1} and other radicals.

In summary, the hydrocarbon plasma during the GDP deposition is investigated. The reactive species are measured by mass spectrum. The results show that the ratio of large-mass species and small-mass species could be controlled. Due to the relationship between hydrocarbon plasma and properties of the GDP shells, the properties of the GDP shells could also be controlled.

2.3. HGM prepared by depolymerizable mandrel technique

With its own advantages like excellent symmetry, sound surface quality, large strength and mediate permeation to hydrogen isotope, thus the preparation of HGMs attracts nonstop research interests. We have commenced to explore a new approach to make HGMs since 2014, which was firstly reported by the National Ignition Campaign (NIC) in the USA [25]. As illustrated in Fig. 5, there are two decisive steps within the process. First, Si:GDP coating with necessary thickness and Si content must be deposited on PAMS mandrels by chemical vapor deposition (CVD) method as depicted in Fig. 5. Afterwards, the prepared PAMS/Si:GDP shell is sintered in a programmable oven from ramping temperatures to as high as 1000 °C with optimized ramping rate and holding time at certain temperatures. After this procedure, the PAMS mandrel is pyrolyzed away, and the Si:GDP shell is oxidized to a glass shell [26,27]. As reported, it is promising to produce HGMs with the diameter ranging from hundreds of micrometers to several millimeters. Moreover, this method is also capable of making HGMs with varied wall thickness.

Recently, the last two steps displayed in Fig. 5 have been simplified into one step. Xu et al. investigated the effects of TMS flow rate and working pressure adopted during the process of Si:GDP deposition, and the sintering program on the shrinkage behavior of shell thickness and diameter, sphericity, composition, surface roughness and gas retention [28,29]. The shrinkage of the diameter and wall thickness of HGM is improved, and the surface roughness decreases with increasing silicon concentration. It is found that too high silicon concentration may lead to a brittle shell which shatters during the sintering process. We have found that 5% silicon in silicon-doped GDP shells is a compromised concentration for fabricating HGMs with 400–600 μm diameters and 5–15 μm thicknesses.

The composition of the HGM shells includes three elements: carbon, silicon and oxygen, and the carbon concentration of the samples decreases significantly, while the silicon concentration increases significantly and it mainly exists in the form of Si–O bonding after the sintering step. After 24 h of deuterium (1.23 MPa) injection, the residual pressure reaches 77.05% in the shells with a diameter of 500 μm and a thickness of 10 μm, and the residual pressure can reach 72.95% after 96 h. It means that the retention property of these HGM shells is excellent and could satisfy the ICF experimental requirements.

The silicon concentration of the shells increases with increasing holding time at 450 °C, while the carbon concentration of the shells decreases. Longer holding time is beneficial to break Si–C chemical bonds and helpful to reduce the remained carbon within the shells. Moreover, the longer holding time is beneficial to form Si–O chemical bonds when ensuring adequate oxygen in the oven, thus increasing the content of SiO_2 of the shells to the greatest extent. It is found that proper extension holding time at 450 °C is helpful to break C=C and C–C bonds. Thus it can minimize the forming of C–Si bonds and the remained carbon within the shells, then we can get high quality HGMs with transparent surface. The surface roughness of the HGMs decreases with increasing holding time at 450 °C during the conversion of Si:GDP to glass. While the wall thickness uniformity of the HGM increases with increasing holding time, the holding time has a minimal impact on the sphericity of the HGMs.

Eventually, we mastered the integral process to prepare HGMs by this new technique. At present, as presented in

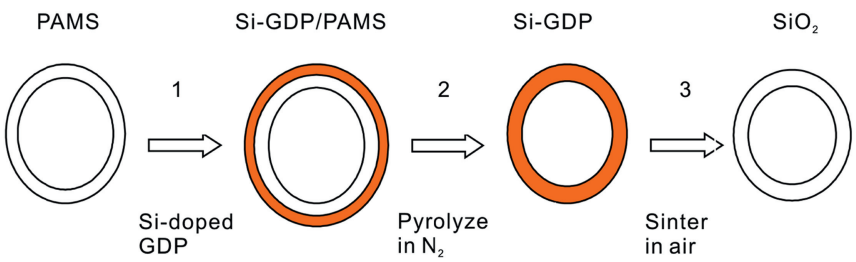

Fig. 5. Fabrication process of an HGM by Si:GDP method.

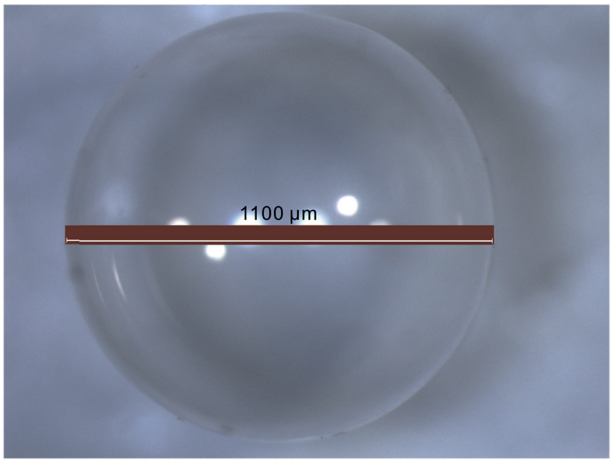

Fig. 6. Photograph of an HGM made by Si:GDP method.

Fig. 6, we are capable of fabricating HGMs with wall thickness ranging from ~5 μm to ~20 μm, and diameter ranging from ~500 μm to ~1.5 mm. As confirmed by the X-ray fluorescence (XRF) analysis displayed in Fig. 7, the gas (Ar), which is utilized as diagnostic element in some ICF experiments, is also filled inside the glass shell simultaneously along the sintering process.

3. Target characterization and assembly

3.1. Measurement of fuel pressure in microsphere of ICF target by white-light interferometry

Nuclear fuel pressure is an essential parameter to estimate fusion efficiency in ICF physical experiments. In fact, the low-*Z* fuel gas is easy to diffuse through the shell. Therefore, fuel pressure should be measured close to the spot time of ICF experiments. However, it is extremely difficult to measure fuel pressure because of very limited access, relatively short optical path length (OPL) changes, and shell expansion after pressurization. As we know, some nondestructive methods such as liquefaction, Raman spectrum analysis, and beta-particle counting have been developed to measure the fuel pressure. However, it takes long time to make deuterium liquefy, so the measurement efficiency of the liquefaction method is too low. The measurements by the Raman method are easily affected by spectral absorption and diffraction in the shell materials. The beta-particle counting method is only suitable for measuring tritium pressure in glass microspheres with relatively thin wall. The destructive methods mainly include the bubble and bursting methods, which are usually used to calibrate parameters for nondestructive methods [30,31]. Therefore, the present methods are not suitable for rapid and nondestructive characterization of fuel gas pressure in ICF experimental targets [32−34]. Some methods of mass spectrometry can measure only the half-life of gas retention [35].

To obtain the fuel pressure for our applications, we propose a method to measure the fuel pressure in the microsphere using vertical scanning white-light interferometry and the proposed expansion model. The basic theory is that the refractive index of fuel gas (n) is obtained by determining the inner diameter (d) and its optical path length (OPL) (L) at the north/south poles of the inner surface for a given orientation before and after pressurization. Since the OPL is very close to the inner surface diameter, the measurement process is realized by the vertical scanning interferometry (VSI) due to its nanometer resolution [36]. The schematic diagram is shown in Fig. 8. When the piezoelectric (PZT) stage moves a minor step, a charge-coupled-device (CCD) camera collects an interference image simultaneously. After the PZT stage moves a certain distance, a group of interference images can be collected. The interference intensity can reach a maximum when the OPL is the same between the reflecting surface and the reference mirror. A data-processing program picks up the interference curve along the vertical scanning direction at the center pixel of each interference pattern. The Hilbert

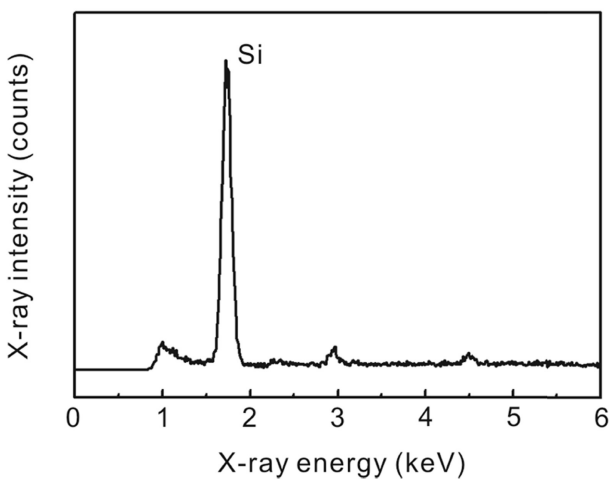

Fig. 7. XRF spectrum of an argon filled Si:GDP.

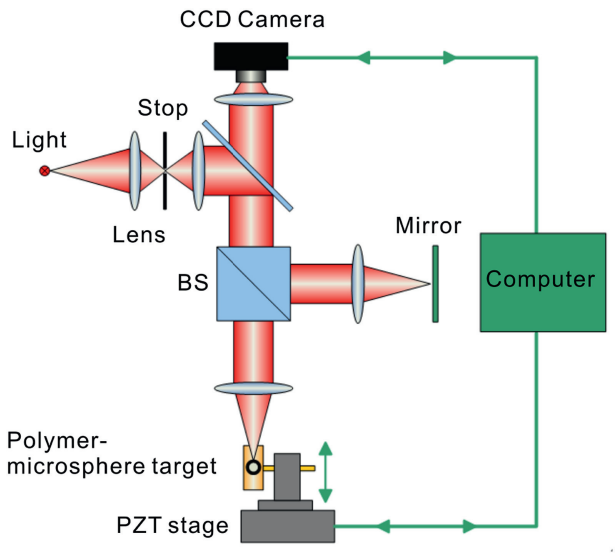

Fig. 8. Schematic diagram of fuel gas OPL measurement in the microsphere.

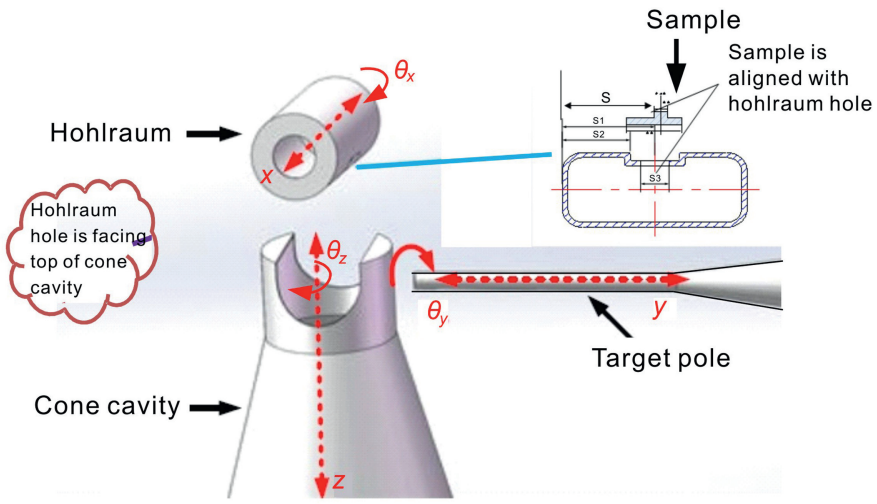

Fig. 9. Sketch map of cavity-cone target.

transform is utilized to obtain the envelope of the interference curve. And then, the diameter of the inner surface or its OPL between the north and south poles on the inner surface of the microspheres can be obtained with a peak searching algorithm based on quadratic fitting. In fact, the refractive index (n) is related not only to the OPL of the fuel gas but also to the expansion (Δd) in the diameter due to pressurization. A theory model is developed to calculate expansion Δd based on classical elasticity theory for hollow spheres. A series of displacement and stress equations are established for all of the homogeneous shell walls under the action of hydrostatic pressure.

To confirm the accuracy of the measurement, the fuel pressure was also measured by the bubble methods. The bubble method is a simple destructive method. The microspheres filled with fuel gas are crushed inside glycerine, and then, the fuel gas forms a large bubble and rises to the glycerine surface. At this time the gas pressure in the bubble is equal to the atmosphere pressure. The diameter of the bubble is measured by a microscope. Based on the state equation of gas, the fuel gas pressure can be easily obtained. The pressure uncertainty for the bubble method is less than 5%. The measurement results show that the white-light interferometry agrees with the bubble method measurements within a 10% deviation. The uncertainty is analyzed to be less than 10% ($k = 2$) for both the glass and the polymer microsphere targets.

In these years, this technique has been successfully applied in the physical experiments of SGIII. This technique is suitable for transparent microspheres such as glass/CH and PS/PVA/CH microspheres. For some nontransparent metal microspheres, we are establishing a laser ultrasonic resonance technique to measure the fuel pressure.

3.2. Assembly method of cavity-cone target

Precise physical experiments are necessary for ICF development, including experiments for hohlraum physics research, shock wave research, radiation transport research,

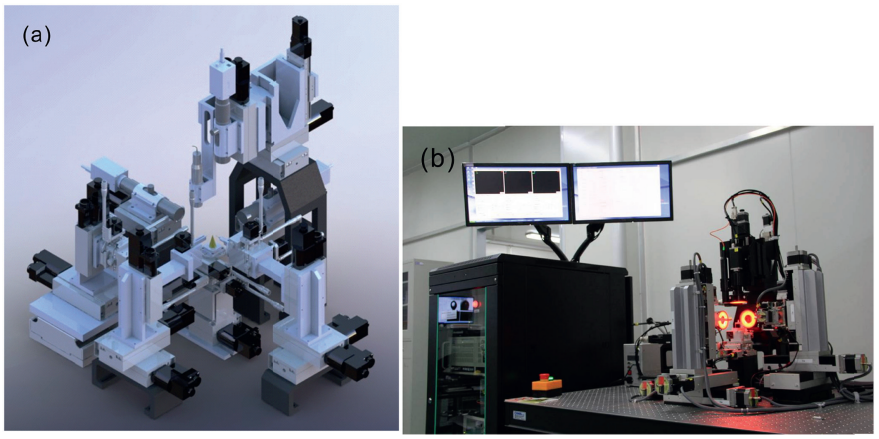

Fig. 10. (a) Diagram and (b) picture of the assembly system.

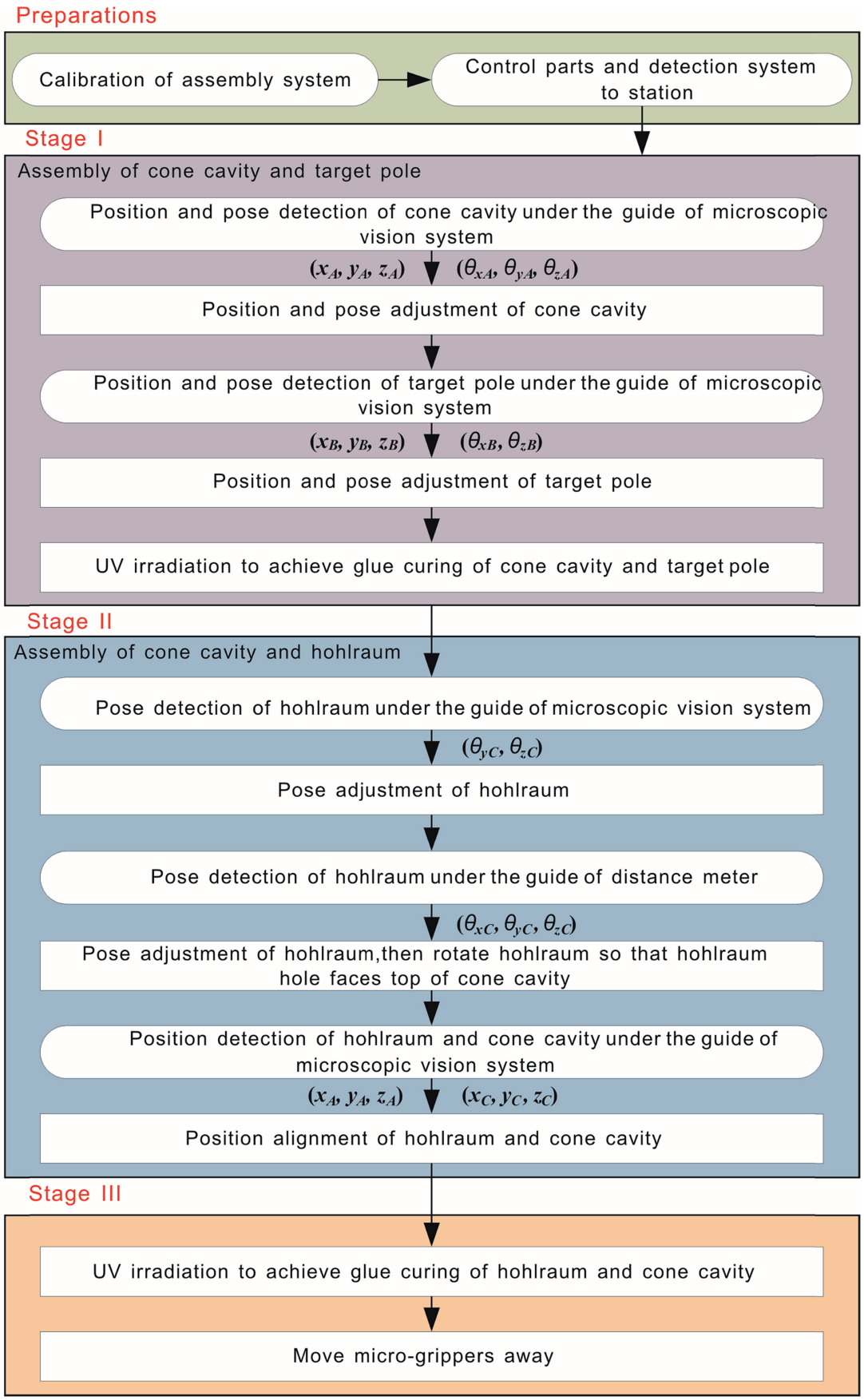

Fig. 11. Diagram of semi-automatic assembly process.

radiative opacity research, and so on. In the precise physical experiments, cavity-cone target is frequently used (shown in Fig. 9). As shown in Fig. 9, the cavity-cone target is composed of a hohlraum, a cone cavity, a sample, and a target pole. There is a hole in the middle of the hohlraum for placing samples. To assemble the target, first, a sample is glued to the hohlraum hole. Then the target pole is aligned with the cone cavity and bonded to the cavity, and the hohlraum is aligned with the cone-shaped cavity. After that, the hohlraum is rotated so that the hohlraum hole faces the top of cone cavity, and finally, the hohlraum is glued on the top of the cone cavity. Since the assembly accuracy of pose and position is highly required, it is difficult to meet the requirement on target accuracy and consistency by manual assembly under the guide of microscope vision or CT. Therefore, a semi-automatic assembly system for the cavity-cone target is developed in laboratory.

Fig. 10(a) shows the 3-D structure of a semi-automatic assembly system for cavity-cone target. It is composed of the detection system, micro-manipulator system, micro-grippers, and control system. The detection system includes vision detection system and distance meter, while the vision detection system includes three microscopic vision systems which are parallel to the x-axis, y-axis, and z-axis, respectively. It is used to detect the relative position of micro-parts in 3-D space and relative pose (θ_y, θ_z). The distance meter is parallel to the z-axis. It is used to detect pose θ_x of the hohlraum hole. To make the normal vector of the hohlraum hole parallel to the z-axis, the pose of the hohlraum is adjusted according to the detection result. A picture of the assembly system is shown in Fig. 10(b).

The micro-manipulator system contains three micro-manipulators. They are used to adjust the position and pose of the hohlraum, cone-shaped cavity, and target pole, respectively. The micro-grippers are used to grip micro-parts in the assembly process. The control system is used to receive detection information, send control commands, and control the assembly process.

The semi-automatic assembly process is divided into four stages (shown in Fig. 11). The preparation stage is to control the micro-parts and detection system movement to the initial station; Stage I is to assemble the target pole and cone cavity; Stage II is to assemble the cone cavity and hohlraum; The last stage—stage III is to move the micro-grippers away after glue curing.

Images in the semi-automatic assembly process are shown in Fig. 12. Fig. 12(a) is an image after adjusting the hohlraum pose. Fig. 12(b) is taken after adjusting the cone-shaped cavity pose. Fig. 12(c) demonstrates the process of hohlraum and cone cavity alignment. Fig. 12(d) shows the image in the process of the cone cavity and target pole alignment, where glue is at the end of the target pole. Fig. 12(e) is the after-assembly image.

The target images after assembly are shown in Fig. 13. We can see that the surface of the target is clean and tidy, and the target shows no deformation. Fig. 14 shows two images of the target shot by CT.

Ten targets have been assembled by the system and measured by CT. The angle α between the central axis of the target pole and the sample surface is measured, and the results are listed in Table 1. The maximum angle error is 1.38°. The deviation d between the sample center line and the cone cavity center line is measured, and the results are listed in Table 2. The maximum deviation in ten groups is 9 μm.

Moreover, the time to achieve a target assembly is less than 30 min. Therefore, the semi-automatic assembly system can be used to assemble cavity-cone targets in high precision and acceptable efficiency.

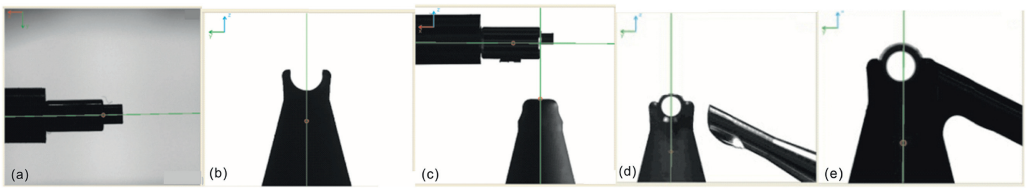

Fig. 12. Images in the micro-assembly process.

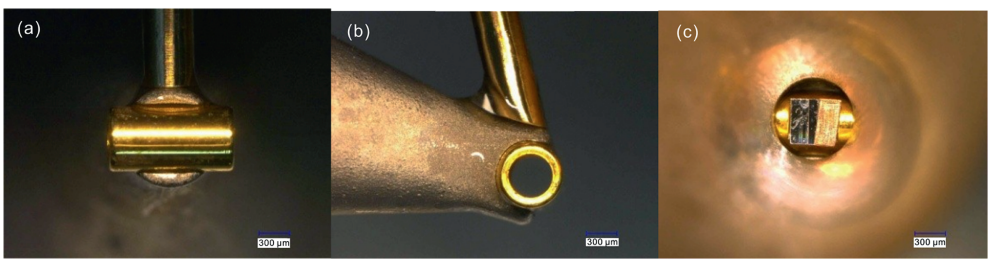

Fig. 13. Images of the micro-target.

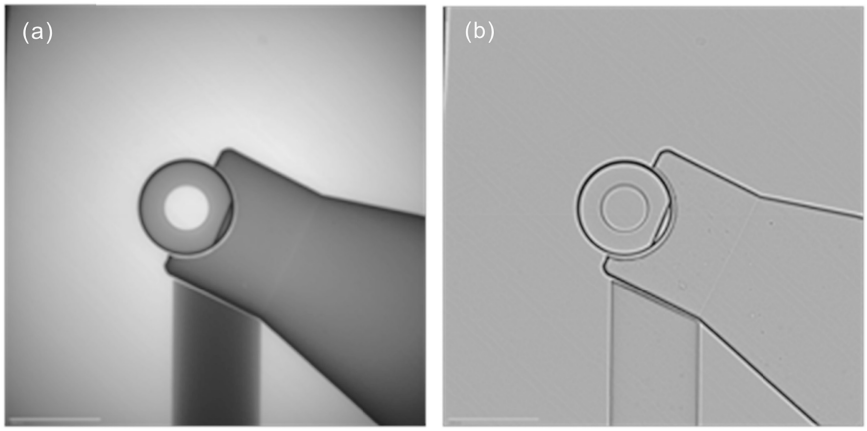

Fig. 14. Images of the micro-target by CT.

Table 1
Target angle error.

Order number	1	2	3	4	5	6
α	24.82°	25.27°	24.62°	26.49°	25.35°	26.20°
Angle error	1.18°	0.73°	1.38°	0.51°	0.65°	0.20°
Conclusion	The maximum angle error is 1.38°					

Table 2
Target position error.

Order number	1	2	3	4	5	6	7	8	9	10
d (μm)	4.3	4.0	2.8	4.3	0.6	9.0	6.4	2.8	3.3	0.7
Conclusion	The maximum position error is 9.0 μm									

4. Conclusions

To improve the quality of the target, both the capsule fabrication techniques for preparing polymer shells—glow discharge polymer (GDP) shells and hollow glass microsphere (HGM)—and the techniques of target characterization and assembly are investigated in this paper. The sphericity and wall thickness uniformity of polymer shells are improved by controlling the deformation of compound droplets during solidifying process, while the properties of GDP shells could be controlled according to the relationship between the hydrocarbon plasma and properties of the GDP shells. Moreover, a new approach based on depolymerizable mandrel technique is also explored to prepare HGM shells. For target characterization and assembly, a new technique based on a vertical scanning white-light interferometry is developed for measuring the fuel pressure in the ICF multiple shell microsphere targets and the semi-automatic assembly system is also developed for precisely assembling cavity-cone targets. With more stringent requirements on the ICF target, more research about the target technique is still needed to be established in the future.

Conflict of interest

The authors declare that there is no conflicts of interest.

References

[1] A.M. Dunne, HiPER: Technical Background and Conceptual Design Report 2007, Science and Technology Facilities Council, Rutherford Appleton Laboratory, Central Laser Facility, 2007.
[2] A.K. Tucker-Schwartz, Z. Bei, R.L. Garrell, T.B. Jones, Polymerization of electric field-centered double emulsion droplets to create polyacrylate shells, Langmuir 26 (2010) 18606−18611.
[3] N. Antipa, S. Baxamusa, E. Buice, A. Conder, M. Emerich, et al., Automated ICF capsule characterization using confocal surface profilometry, Fusion Sci. Technol. 63 (2013) 151−159.
[4] K. Nagai, H. Yang, T. Norimatsu, H. Azechi, F. Belkada, et al., Fabrication of aerogel capsule, bromine-doped capsule, and modified gold cone in modified target for the Fast Ignition Realization Experiment (FIREX) Project, Nucl. Fusion 49 (2009) 095028.
[5] P.R. Paguio, S.P. Paguio, C.A. Frederick, A. Nikroo, O. Acenas, Improving the yield of target quality Omega size PAMS mandrels by modifying emulsion components, Fusion Sci. Technol. 49 (2006) 743−749.
[6] T. Nisisako, Recent advances in microfluidic production of Janus droplets and particles, Curr. Opin. Colloid Interface Sci. 25 (2016) 1−12.
[7] S. Waheed, J.M. Cabot, N.P. Macdonald, T. Lewis, R.M. Guijt, 3D printed microfluidic devices: enablers and barriers, Lab Chip 16 (2016) 1993−2013.
[8] L.R. Shang, Y. Cheng, Y.J. Zhao, Emerging droplet microfluidics, Chem. Rev. 117 (2017) 7964−8040.
[9] X. Qu, Y. Wang, Dynamics of concentric and eccentric compound droplets suspended in extensional flows, Phys. Fluids 24 (2012) 123302−123321.
[10] M.F. Liu, Y.Y. Liu, J. Li, S.F. Chen, J. Li, et al., Improvement of sphericity of thick-walled polystyrene shell, Colloids Surf. A 484 (2015) 463−470.
[11] M.F. Liu, L. Su, J. Li, S.F. Chen, Y.Y. Liu, Investigation of spherical and concentric mechanism of compound droplets, Matter Radiat. Extrems 1 (2016) 213−223.
[12] M.F. Liu, S.F. Chen, X.B. Qi, B. Li, R.T. Shi, et al., Improvement of wall thickness uniformity of thick-walled polystyrene shells by density matching, Chem. Eng. J. 241 (2014) 466−476.
[13] M.F. Liu, Y.Q. Zheng, J. Li, S.F. Chen, Y.Y. Liu, et al., Effects of molecular weight of PVA on formation, stability and deformation of compound droplets for ICF polymer shells, Nucl. Fusion 57 (2017) 016018.
[14] A. Nikroo, J.M. Pontelandolfo, E.R. Castillo, Coating and mandrel effects on fabrication of glow discharge polymer NIF scale indirect drive capsules, Fusion Sci. Technol. 41 (2002) 220−225.
[15] S.A. Letts, D.W. Myers, L.A. Witt, Ultrasmooth plasma polymerized coatings for laser fusion targets, J. Vac. Sci. Technol 19 (1981) 739−742.
[16] D.G. Czechowicz, E.R. Castillo, A. Nikroo, Composition and structural studies of glow discharge polymer coatings, Fusion Sci. Technol. 41 (2002) 188−192.

[17] A. Nikroo, D.G. Czechowicz, E.R. Castillo, J.M. Pontelandolfo, Recent progress in fabrication of high-strength glow discharge polymer shells by optimization of coating parameters, Fusion Sci. Technol. 41 (2002) 214−219.
[18] M. Theobald, B. Dumay, C. Chicanne, J. Barnouin, O. Legaie, et al., Roughness optimization at high modes for GDP CHx microshells, Fusion Sci. Technol. 45 (2004) 176−179.
[19] K.C. Chen, R.C. Cook, H. Huang, S.A. Letts, A. Nikroo, Fabrication of graded germanium-doped CH shells, Fusion Sci. Technol. 49 (2006) 750−755.
[20] L. Zhang, X.S. He, G. Chen, T. Wang, Y.J. Tang, et al., Effects of rf power on chemical composition and surface roughness of glow discharge polymer films, Appl. Surf. Sci. 366 (2016) 499−505.
[21] J.P. Booth, G. Cunge, CF_x radical production and loss in a CF_4 reactive ion etching plasma: fluorine rich conditions, J. Appl. Phys. 85 (1999) 3097−3102.
[22] G. Chen, L. Zhang, X.S. He, Z.B. He, Y.J. Tang, Effect of the gas flow ratio of T_2B/H_2 on the composition and surface roughness of glow discharge polymer films, Atomic Energy Sci. Technol. 9 (2016) 1658−1663.
[23] R.W. Luo, A.L. Greenwood, A. Nikroo, C. Chen, Properties of silicon-doped GDP shells used for cryogenic implosions at OMEGA, Fusion Sci. Technol. 55 (2009) 456−460.
[24] R. Brusasco, M. Saculla, R. Cook, Preparation of germanium doped plasma polymerized coatings as inertial confinement fusion target, J. Vac. Sci. Technol. Vac. Surf. Films 13 (1995) 948−951.
[25] S.A. Letts, E.M. Fearon, S.R. Buckley, M.D. Saculla, L.M. Allison, et al., Fabrication of polymer shells using a decomposable mandrel, Fusion Technol. 28 (1995) 1797−1802.
[26] M.L. Hoppe, Large glass shells from GDP shells, Fusion Technol. 38 (2000) 42−48.
[27] M.L. Hoppe, Recent developments in making glass shells from silicon doped GDP shells, Fusion Sci. Technol. 41 (2002) 234−237.
[28] W. Xu, T. Wang, Z.B. He, Z.W. Wu, Fabrication of hollow glass microspheres for inertial confinement fusion targets depolymerizable mandrel method, High Power Laser Part. Beams 27 (2015) 062008−062015.
[29] W. Xu, T. Wang, Z.W. Wu, Z.B. He, Influence of pressure on structure and properties of hollow glass microspheres, High Power Laser Part Beams 27 (2015) 122004−122010.
[30] W. Rensel, T. Henderson, D. Solomon, Novel method for measuring total pressure of fuel gas in hollow, glass microshell pellet, Rev. Sci. Inst. 46 (1975) 787−789.
[31] M. Salazar, P. Gobby, R. Watt, Pressure testing of micro balloons by bursting, Fusion Technol. 38 (2000) 136−138.
[32] J. Sanchez, R. Upadhye, Non-destructive method for measuring the D_2/DT fill pressure and permeability for direct drive plastic shells, Nucl. Fusion 31 (1991) 459−464.
[33] S. Ohira, H. Akamura, S. Konishi, T. Hayashi, K. Okuno, et al., On-line tritium process gas analysis laser Raman spectroscopy at TSTA, Fusion Technol. 21 (1992) 465−470.
[34] H. Deckman, G. Halpern, Fuel content characterization and pressure retention measurements of DT-filled laser fusion microballoon targets, J. Appl. Phys. 50 (1979) 132−139.
[35] D. Steinman, E. Alfonso, M. Hoppe, Developments in capsule gas fill half-life determination, Fusion Sci. Technol. 5 (2007) 544−546.
[36] Z. Wang, D. Gao, X. Ma, J. Meng, White-light interferometry for measuring fuel pressure in ICF polymer-microsphere targets, Fusion Sci. Technol. 66 (2014) 432−437.